Formation and Characterization of Ni Nanostructures in Porous InP – from Crystallites to Wires

M.-D. GERNGROSS*, V. HRKAC, L. KIENLE, J. CARSTENSEN, and H. FÖLL
Institute for Materials Science, Christian-Albrechts-University of Kiel,
Kaiserstrasse 2, 24143 Kiel, Germany
* *mdg@tf.uni-kiel.de*

***Abstract* — In this work the galvanic formation of Ni crystallites and Ni nanowires with very high aspect ratios (>1000:1) in porous InP is presented. By depositing a dielectric interlayer on the InP pore walls it is possible to produce very high aspect ratio Ni nanowires. The coercivity of these nanowires is about 100 Oe (in-plane) and 240 Oe (out-of-plane), while the coercivity of the crystallites lies in between these values. The in-plane remanence squareness of the Ni nanowires is very low (S ≈ 0.08), out-of-plane it is 0.36. For the Ni crystallites the remanence squareness lies in between the range given for the Ni nanowires.**

***Index Terms* — indium phosphide, porous, galvanic deposition, nickel.**

I. INTRODUCTION

In the present work the galvanic fabrication of Ni crystallites and nanowires in porous InP is described and their structural and magnetic properties are discussed. The combination of a piezoelectric and a magnetostrictive material produces a multiferroic composite with unusual properties that can be used, e.g., for magnetoelectric sensors [1].

As piezoelectric component InP is used for this composite material. InP is a III-V compound semiconductor with poor bulk piezoelectric properties [2, 3]. The piezoelectric properties of InP can be highly increased (factor of 30) by producing a self-organized, hexagonally close-packed array of current-line pores with completely overlapping space charge regions (SCR) by electrochemical etching and post-etching [4].

To fabricate a multiferroic 1-3 composite it is necessary to deposit a magnetostrictive material – such as Ni – inside the porous InP. In principle, this can be done by atomic layer deposition (ALD) and galvanic deposition. The major disadvantages of ALD are the extremely long processing time for thick films and the huge problems in the deposition of metal films, which – on the other hand – can be easily overcome by galvanic deposition. Nevertheless, the galvanic deposition of metals and alloys in very high aspect ratio semiconductor pores is a very sophisticated process, although the galvanic deposition of metals has been widely investigated for porous alumina [5, 6]. Granitzer et al. have deposited Ni crystallites inside a very high aspect ratio Si pore array, but it has not been possible to grow dense nanowires homogeneously from the pore tip [7, 8]. Tiginyanu et al. have shown for InP pore arrays that it is possible to coat the pore walls homogeneously with Pt resulting in Pt nanotubes embedded in an InP pore array, but nanowires could not be obtained [9]. A possible reason is the leakage current through the InP pore walls allowing the nucleation of metal clusters directly on the pore walls. Thus a thin dielectric interlayer is deposited on the pore walls preventing a leakage current flow through the pore walls. By applying this concept solid Ni nanowires with very high aspect ratios of about 1000:1 embedded in an InP membrane could be grown. Without this dielectric interlayer roundish Ni crystallites are deposited on the InP pore walls.

II. EXPERIMENTAL

In this work single-crystalline (100) oriented InP wafers were used, doped with S at a doping carrier concentration of $1.1 \cdot 10^{17}$ cm^{-3} and a resistivity of 0.019 Ω cm. Two different samples were produced, an InP pore array and an InP membrane. InP wafers with two different thicknesses are used, 500 µm ± 10 µm and 400 µm ± 10 µm, respectively. The wafers were double-side polished. The sample size was $A = 0.25$ cm² in both cases.

The first step is the formation of so-called current-line oriented pores (curro-pores) in a self-organized highly regular array [10]. This is done by electrochemical etching in an electrochemical double cell [11] using a 6 wt.% aqueous HCl electrolyte at 20 °C. A homogeneous nucleation of the curro-pores is achieved by applying a high voltage pulse for the first second, followed by a constant anodic etching potential. In the case of the pore array the etching time is 1.5 min, while it is 41 min for the membrane.

The membrane is obtained by opening the bulk back side in a two-step etching process combining photoelectro-chemical and photochemical etching in 6 wt% at 20 °C. This etching process is described in detail in [12].

The next step is the post-etching of the InP pore array and membrane. This step is necessary to produce overlapping SCR around each pore. Since no free charge carriers are present in the SCR, the conductivity of the InP pore walls can be highly reduced. For the post-etching, an $HF:HNO_3$:EtOH:HAc (3:8:15:24) based electrolyte is used. It is kept at 20 °C during the entire

post-etching time. In the case of the pore array, the post-etching is performed under open circuit conditions for 48 h, while the membrane is post-etched under a cathodic bias of –0.8 V for 17 h. Afterwards the samples are thoroughly rinsed in deionized water and air-dried.

To avoid unfavorable current flow through the pore walls, an 8 nm layer of Al_2O_3 is deposited on the pore walls of the InP membrane. This dielectric layer is formed by 80 cycles of trimethylaluminum (TMA) and H_2O at 300 °C in a Picosun Sunale R200 ALD tool. To achieve homogeneous wall coverage in the very high aspect ratio membranes the diffusion time of the gases is extended.

The galvanic Ni deposition is performed in an electrochemical cell with a three-electrode configuration: a Pt counter electrode, a Pt pseudo-reference electrode (both immersed into the electrolyte), and the working electrode. In case of the InP pore array the pore array itself is the working electrode, while for the membrane, a 400 nm Au layer that is sputter-deposited on the back side of the membrane is acting as working electrode. Using this thick Au layer ensures that the back side is completely covered with Au. The Ni electrolyte is a typical Watt's type with a *p*H value adjusted to around 3. The electrolyte temperature is 20 °C for the pore array and 35 °C for the membrane. In the case of the pore array the current density of 20 mA/cm² is applied in pulses of 0.8 s with a recovering time of 4.6 s, while for the InP membrane the current density of 17 mA/cm² is applied constantly. For both cases the Ni deposition time is 60 min.

Both composite structures were investigated using an FEI Helios D477 SEM and a Seifert XRD 3000 TT (Cu $K_{\square}$ = 0.154 nm). For the structural investigation TEM was performed using a Tecnai F30 STwin microscope (300 kV, field-emission gun, spherical aberration constant Cs = 1.2mm). For the preparation of the specimens a conventional method was applied: two face-to-face bonded films were mechanically thinned and subsequently ion milled (PIPS). The magnetic properties were investigated using a LakeShore 7300 vibrating sample magnetometer (VSM).

III. RESULTS & DISCUSSION

Structural properties

Figure 1 (a) presents the cross-sectional view on the InP pore array after Ni deposition. The aspect ratio of the pores obtained after electrochemical etching and post-etching is about 500:1. One observes a high density of Ni crystallites on the pore walls. Due to the pulsed deposition with high recovering time no plugging of the pore openings is observed. The Ni crystallites seem roundish and almost of equal size. The average Ni crystallite size is around 50 nm determined from SEM images. They are homogeneously distributed along the complete length of the pore. At several positions, these crystallites have grown into each other forming a tubular structure – as shown in the left part of the inset of Fig. 1 (a). This growth behavior is very similar to the Pt tube grown in highly doped InP pore arrays obtained by Tiginyanu et al. [9].

In Fig. 1 (b) the cross-sectional view on the InP membrane filled with Ni nanowires is depicted. The aspect ratio of the membrane after electrochemical etching and cathodic post-etching is about 1600:1. The nanowires were grown from the Au plating base to the top. Since they were produced in a membrane consisting of rectangular pores, they exhibit a rectangular shape with a typical aspect ratio of about 1000:1. The distance between neighboring wires is about 100 nm. Similar to the Ni crystallites in Fig 1 (a) the Ni nanowires appear bright in the SEM if they are broken and partially sticking out of the membrane. These fractures originate only from the sample cleavage and are not a property of the nanowires themselves. The two SEM images show impressively that the use of a thin dielectric interlayer consisting of Al_2O_3 prevents efficiently the current flow through the pore walls and thus allows a homogeneous formation of solid nanowires.

The XRD pattern of the Ni crystallites deposited inside the InP pore array is presented in Fig. 2 (a). It shows one InP peak and three peaks that can be assigned to Ni with the fcc crystal structure. The Ni peaks are indexed as Ni{111}, Ni {200} and Ni {220}. The {110} peak is almost suppressed. From the peak broadening the Ni crystallite size can be calculated by the Scherrer formula. The average crystallite size obtained from all three Ni crystal peaks is about 10 nm. The difference in crystallite size compared to the result obtained from SEM images can be explained by oxidation of the Ni crystallites leaving a much smaller crystalline Ni crystallite. Since the Ni crystallites have a high surface area compared to their volume they can oxidize easily. This oxidization results in the formation of a crystalline Ni_2O_3 phase indicated by the additional Ni_2O_3 peaks in the XRD pattern. The peak indexed with the asterisk cannot be assigned to Ni, all kinds of Ni oxide, or InP. Most probably this is an artifact.

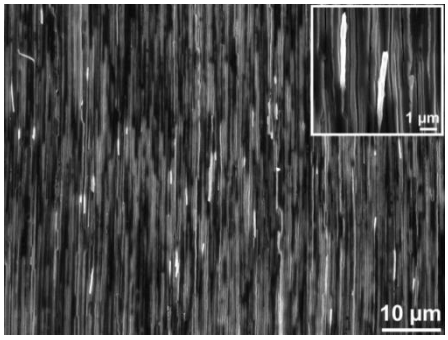

(a)

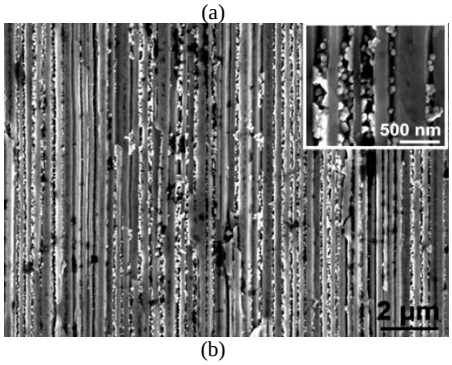

(b)

Fig. 1 Cross-sectional view on the (a) InP pore array with Ni crystallites, inset: high magnification of Ni crystallites, and (b) InP membrane with Ni nanowires, inset: high magnification image of single Ni nanowires.

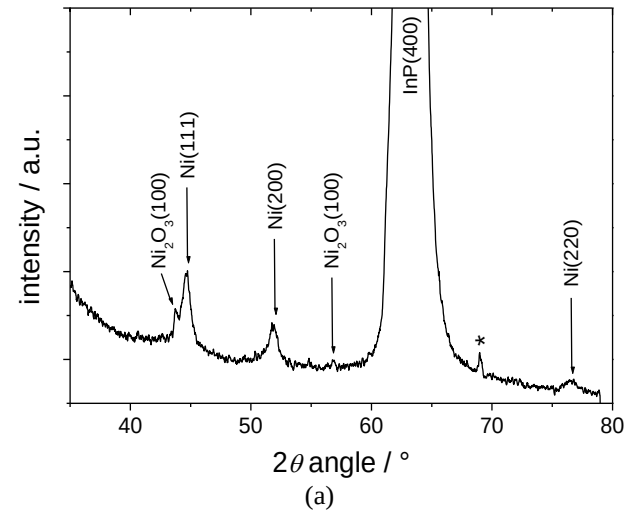

(a)

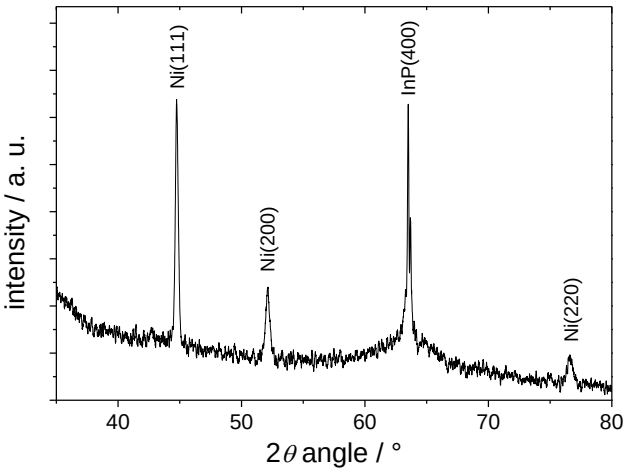

(b)

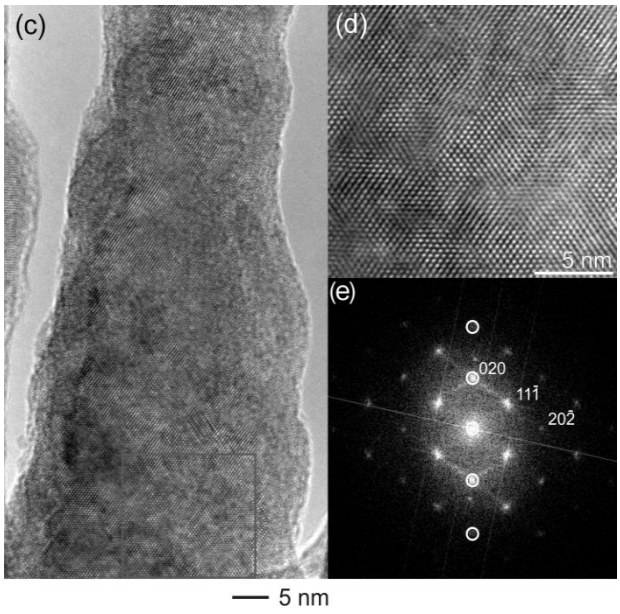

Fig. 2 XRD patterns of (a) Ni crystallites embedded in the InP pore array and (b) Ni nanowires embedded in the InP membrane. (c) HRTEM micrograph of an InP pore wall, (d) magnified and filtered [13] view of the marked area with (e) associated FFT along the zone axis [101]. The marked intensities indicate the growth direction <100>.

In Fig. 2 (b) the XRD pattern of the Ni nanowires embedded into the InP membrane is depicted. It shows that the nanowires are not single-crystalline. The three single Ni peaks are much sharper compared to the Ni peaks of the embedded Ni crystallites. Additionally, the Ni {220} peak is more pronounced compared to the corresponding peak of the Ni crystallites. In contrast to the Ni crystallites, the Ni {111} and the Ni {200} peaks are as sharp as the InP {400} peak, which indicates rather large coherently scattering areas. The crystal size is determined from the Scherrer formula. It is about 20 nm for the Ni {200} and {220} peak, while it is about 60 nm for the Ni {111} peak. This is an indication for a slight {111} texture of the Ni nanowires, discussed in the magnetic properties section in more detail.

The crystallinity of the InP pore array was additionally investigated by high resolution TEM (HRTEM). The resulting images are presented in Fig. 2 (c)-(e). Figure 2 (c) gives a typical cross-sectional view on the pore wall with the InP pore wall in the center of the image. The FFT along the zone axis [101] – depicted in Fig. 2 (e) – of the selected high magnification view [Fig. 2 (d)] reveals the expected single-crystalline zinc blende structure of the InP with the growth direction parallel to <100>.

Magnetic properties

The magnetic properties of the Ni crystallites and Ni nanowires are investigated by in-plane ($\alpha = 0°$) and out-of-plane ($\alpha = 90°$) VSM measurements.

For the Ni nanowires additional hysteresis loops were measured in 15° steps between in-plane and out-of-plane orientation. Here in-plane means, the magnetic field is parallel to the sample surface, but perpendicular to the Ni nanowires. Since the Ni nanowires have a rectangular cross-sectional area, also in-plane hysteresis loops under angles from 0° to 90° in 15° steps are performed.

In Fig. 3 (a) the hysteresis loops for Ni crystallites are shown. The in-plane ($\alpha = 0°$) hysteresis loop is narrow. The coercivity H_C is about 125 Oe and the remanence squareness S is about 0.12. Compared to the in-plane hysteresis loop, the out-of-plane ($\alpha = 90°$) hysteresis loop is much broader and the slope around H_C is much steeper. The coercivity is around 218 Oe and the remanence squareness increases to about 0.33.

In Fig. 3 (b) the hysteresis loops of the Ni nanowires are presented. It is found that the hysteresis loops broaden as well and the slope around H_C steepens with increasing angle α. Compared to the in-plane hysteresis loop of the Ni crystallites, the in-plane hysteresis loop of the nanowires is even narrower. The coercivity H_C is about 100 Oe. The remanence squareness S is about 0.08. According to [14], this indicates an almost perfect alignment of the easy axis of the Ni nanowires parallel to the long wire axis. Compared to the in-plane hysteresis loop, the out-of plane hysteresis loop is much broader. The coercivity is about 240 Oe and the remanence squareness increases to about 0.36 indicating a rather random distribution of the easy axis in parallel to the surface.

The resulting in-plane hysteresis loops are shown in the inset of Fig. 3 (b). No change in the hysteresis loops is found, showing that the magnetic properties of the Ni nanowires are independent of the rectangular wire cross-section.

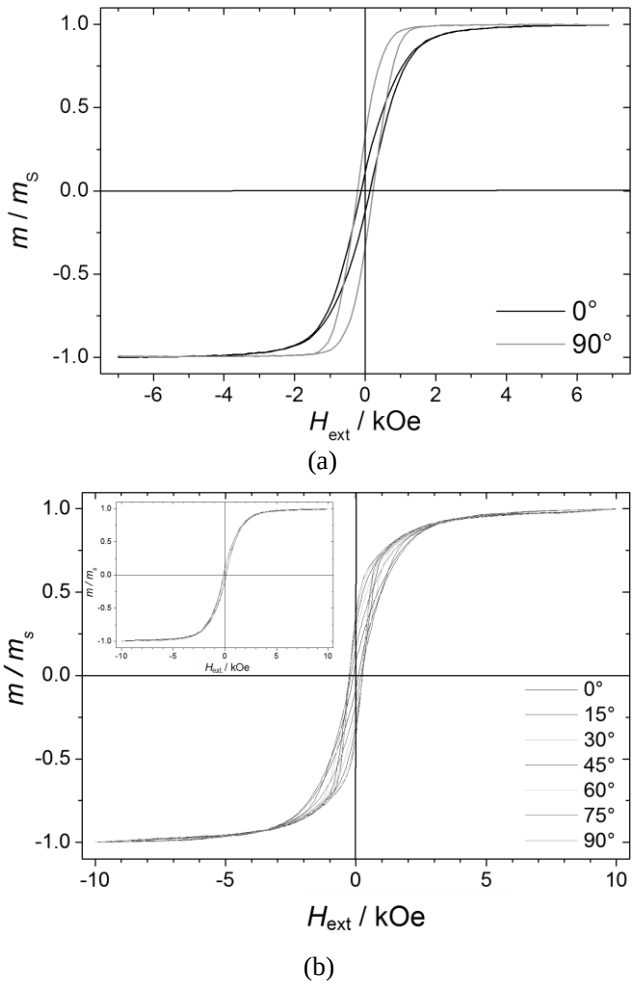

Fig. 3 Hysteresis loops of (a) Ni crystallites embedded in the InP pore array measured in in-plane (0°) and out-of plane, (b) Ni nanowires embedded in an InP membrane measured between in-plane and out-of-plane in 15° steps. Inset: angular dependence of in-plane hysteresis loops under various in-plane angles of the magnetic field with respect to the Ni nanowires.

SUMMARY & CONCLUSION

The formation of Ni crystallites and solid Ni nanowires by galvanic deposition in very high aspect ratio porous InP structures has been shown. In order to obtain solid nanowires it is beneficial to homogeneously coat the porous InP with a thin dielectric interlayer of Al_2O_3. Roundish Ni crystallites could be obtained by pulsed galvanic deposition in InP pores without an interlayer. In both cases the resulting Ni structures are crystalline. The magnetic properties obtained in both deposition procedures are very similar. In general the hysteresis loops of the Ni crystallites are much broader and more rectangular compared to the Ni nanowires. The remanence squareness of the Ni crystallites is not as pronounced as for the nanowires, which also applies to the coercivity. It was also found that the rectangular cross-sectional area has no influence on the magnetic properties of the Ni nanowires.

ACKNOWLEDGEMENTS

This work was funded by the collaborative research center 855 “Magnetoelectric Composites – Future Biomagnetic Interfaces” by the DFG. Special thanks goes to Dr. E. Quiroga-González for recording the XRD patterns.

REFERENCES

[1] J. Zhai, Z. Xing, S. Dong, J. Li, and D. Viehland, *Appl. Phys. Lett.* **88**, 062510 (2006).
[2] K. Rottner, R. Helbig, and G. Müller, *Appl. Phys. Lett.* **62(4)**, 352 (1993).
[3] G. Arlt and P. Quadflieg, *Phys. Status Solidi.* **25**, 323 (1968).
[4] M.-D. Gerngross, V. Sprincean, M. Leisner, J. Carstensen, H. Föll, and I. Tiginyanu, *ECS Trans.* **35(8)**, 67 (2011).
[5] K. Nielsch and B.J.H. Stadler, "Template-based synthesis and characterization of high-density ferromagnetic nanowire arrays", in Handbook of Magnetism and Advanced Magnetic Materials, eds. H. Kronmüller and S. Parkin, 2227-2255, John Wiley & Sons, London (2007).
[6] N. Lupu, H. Chiriac, and P. Pascariu, *J. Appl. Phys.* **103**, 07B511 (2008).
[7] K. Rumpf, P. Granitzer, P. Pölt, S. Simic, and H. Krenn, *Phys. Status Solidi (a)* **205(6)**, 1354 (2008).
[8] P. Granitzer, K. Rumpf, P. Pölt, S. Simic, and H. Krenn, *Phys. Status Solidi (c)* **5(12)**, 3580 (2008).
[9] I. Tiginyanu, E. Monaico, and E. Monaico, *Electrochem. Comm.* **10(5)**, 731 (2008).
[10] M. Leisner, J. Carstensen, and H. Föll, *Nanoscale Res. Lett.* **5(7)**, 1190 (2010).
[11] S. Langa, I.M. Tiginyanu, J. Carstensen, M. Christophersen, and H. Föll, *Electrochem. Solid-State Lett.* **3(11)**, 514 (2000).
[12] M.-D. Gerngross, J. Carstensen, and H. Föll, *J. Electrochem. Soc.* **159(11)**, H857 (2012).
[13] R. Kilaas, *Journal of Microscopy* **190**, 45-51 (1998).
[14] J.M.D. Coey, *Magnetism and magnetic materials*, Cambridge University Press, Cambridge (2005).